CONFERENCE PRE-PRINT

GLOBAL DISPERSION AND NONLINEAR DYNAMICS IN PLASMAS MODELED FOR JT-60U STRONGLY REVERSED MAGNETIC SHEAR CONFIGURATION EXHIBITING A SIGNATURE OF ITBS FROM L-MODE CHARACTERISTICS

R. ZHAO, K. Imadera, J.F. Liu, A. Ishizawa, Y. Kishimoto Graduate School of Energy Science, Kyoto University Uji, Kyoto, Japan Email: zhao.rui.27d@st.kyoto-u.ac.jp

W. Wang, J.Q. Li Southwestern Institute of Physics Chengdu, People's Republic of China

Z.X. Wang Dalian University of Technology Dalian, People's Republic of China

Abstract

The global dispersion of unstable drift modes and associated turbulent transport is investigated through δf -based global gyrokinetic simulations, modeled for JT-60U strongly reversed magnetic shear (RS) plasmas, exhibiting L-mode characteristics with constrained profiles dominated by large-scale avalanches. Owing to the distinct profiles of ion/electron temperatures and density, two different branches with respect to the toroidal mode number n are identified, mapped onto the radius r. One is the density gradient driven trapped electron modes (∇n -TEMs) in the inner region with lower n values. As n increases, they transit to *ubiquitous modes* and then to toroidal *ion temperature gradient* (ITG) modes, while the other branch corresponds to the slab-like non-resonant ITG modes at higher n values, all localized at the minimum q (q_{min}) surface. Here, the maximum growth rates in each branch are almost the same, i.e. $\gamma_{max}^{in} \sim \gamma_{max}^{out}$, indicating that unstable free energy sources are configured to be globally balanced, preventing unbalanced transport between the inner and outer regions. Correspondingly, the turbulence is initiated from both inside $(r \sim r_{in})$ and outside $(r \sim r_{min})$. Then, each of them spread to both sides coupled with geodesic acoustic modes (GAMs), generating three regions, i.e., [A] the inside region ($r \le r_{in}$), [B] the intermediate region $(r_{in} \le r \le r_{min})$, and [C] the outside region $(r \ge r_{min})$. In region [B], turbulence from both directions coalesces, forming a novel state coupled with counter propagating GAMs. In region [C], the turbulence excited near q_{min} surface transfers energy to propagating GAMs. With associated oscillating radial electric field E_r and its radial gradient $(\partial E_r/\partial r)$ advected outward and dissipated, thereby suppressing turbulence. A similar process is found to take place in the inside region [A]. These results indicate that two ITBs can be triggered, one is near the outside of the q_{min} surface, the other is inside of the maximum density gradient, serving as a seed for triggering ITBs consistent with those observed in JT-60U discharge.

1. INTRODUCTION

Reversed magnetic shear (RS) plasmas, where the safety factor profile q has a minimum value q_{min} at a certain radius $r = r_{min}$, have attracted attention, leading to internal transport barriers (ITBs) [1]-[8]. However, even with such non-monotonic q-profiles, plasmas are found to exhibit L-mode characteristics with strongly constrained profiles under the sub-critical input neutral beam injection power, dominated by large scale avalanches, as studied in JT-60U [5][6]. This leads to the conjecture that L-modes are universal without strictly depending on the magnetic structure. Given that the mode distribution is regulated by the q profile via the resonance, $nq \sim m$, it is important to unravel the underlying physics. Based on the understanding of such L-mode plasmas with RS q profile, we revisit the properties of instability free energy sources for plasmas with strongly RS q profiles, modelled for those in JT-60U, as shown in Figs. 1(a) (b), and their nonlinear dynamics based on the simulations using the global gyro-kinetic code (GKNET) [7]-[10]. An interesting feature is that the ion/electron temperature scale lengths L_T and the density scale length L_n are separated, i.e. the maximum of the inverse density scale length (R_0/L_n) is localized in the inner region with negative magnetic shear $(\hat{s} < 0)$ at $r \sim r_{in} (\sim 0.4)$, while those of the temperatures are localized in the outer region around the q_{min} surface with $\hat{s} \sim 0$ at $r \sim r_{min} (= 0.7)$. It should be noted is that, unless otherwise specified, the spatial coordinates (particularly the radial coordinate) are

normalized by the minor radius a_0 throughout the remainder of this article. Due to the presence of different instability free energy sources in different radial locations, multiple branches and associated eigen-modes are thought to exist, which makes the transport process more complicated.

2. NUMERICAL MODEL

Based on the above discussed motivation, δf -based electrostatic gyro-kinetic simulations, including both linear and nonlinear calculations, are performed using the GKNET code [7]-[10], which solves the Vlasov equation in a five-dimensional gyro-center coordinate system $(\mathbf{R}, \mu, \nu_{\parallel})$ for both electrons and ions. The particle index s denotes either the deuterium ion (i) or electron (e). The following equations describe the time evolution of the gyro-averaged distribution function f_s :

$$\frac{\partial}{\partial t}(Jf_s) + J\frac{d\mathbf{R}}{dt} \cdot \frac{\partial f_s}{\partial \mathbf{R}} + J\frac{dv_{\parallel}}{dt} \cdot \frac{\partial f_s}{\partial v_{\parallel}} = 0, \tag{1}$$

Here, $\mathbf{R} \equiv (r, \theta, \phi)$ represents the guiding center position, v_{\parallel} denotes the parallel velocity along the field line, and $\mu = m_s v_{\perp}^2 / 2B$ is the magnetic moment for the particle s.

$$\frac{d\mathbf{R}}{dt} = \frac{1}{B_{\parallel,s}^*} \left[v_{\parallel}(\nabla \times \mathbf{A}) + \frac{B_0}{\Omega_s} v_{\parallel}^2(\nabla \times \mathbf{b}) + \frac{c}{e_s} H_s \nabla \times \mathbf{b} - \frac{c}{e_s} \nabla \times (H_s \mathbf{b}) \right], \tag{2}$$

$$\frac{dv_{\parallel}}{dt} = -\frac{1}{m_{S}B_{\parallel,S}^{*}} \left[(\nabla \times \mathbf{A}) \cdot \nabla H_{S} + \frac{B_{0}}{\Omega_{S}} v_{\parallel} \nabla \cdot (H_{S} \nabla \times \mathbf{b}) \right], \tag{3}$$

where $J=rRB_{\parallel}^*$ is the phase space Jacobian, $B_{\parallel,s}^*=\nabla\times A^*=\nabla\times (A+B_0v_{\parallel}/\Omega_s b)$ is the modified magnetic field for the particle, b=B/B denotes the unit vector in the magnetic field direction, A is the vector potential, $\Omega_s=e_sB_0/m_sc$ is the gyro-frequency, the e_s and m_s represent the charge and mass of the particle s, and s is the speed of light. For geometry, we adopt a circular cross-section and define two-dimensional poloidal cross-section $\mathbf{R}_p\equiv (r,\theta)$ in an axisymmetric system, so that the $=R_0+r\cos\theta$. The reference magnetic field B_0 is defined at the major radius R_0 , $H_s=m_sv_{\parallel}^2/2+\mu B+\langle\phi\rangle_{\alpha,s}$ is the gyro-kinetic Hamiltonian for the s particle, where $\langle\phi\rangle_{\alpha,s}$ is the gyro-averaged electrostatic potential.

The Eq. (1) is self-consistently coupled to the quasi-neutrality conditions $\delta n_i = \delta n_e$ based on the hybrid kinetic electron model [11][12]. In this model, the adiabatic response is assumed for the passing electrons with $(m, n) \neq (0,0)$, while all trapped electron and the (m, n) = (0,0) passing electrons are treated kinetically. This hybrid treatment allows the reproduction of a wide range of ion and electron modes.

3. LINEAR EIGEN-MODE DYNAMICS AND DISTRIBUTION

From the series of simulations, we found qualitatively different two branches and associated modes, as shown in Fig. 1(c) for real frequency ω_r and (d) for growth rate γ with respect to n. One is ballooning type resonant modes with lower-n values for $2 \le n \le 16$ lying in the inner negative magnetic shear region $(r < r_{min}, \hat{s} < 1)$ 0), exhibiting highly localized structure in the poloidal direction, the other is non-resonant modes with higher-n values for $18 \le n \le 44$ lie in the outer region, which are all localized around the q_{min} surface. The former branch is identified as the density gradient driven trapped electron modes (∇n -TEMs) [13][14], which show the largest growth rate at n=4 with positive real frequency ($\omega_r>0$) rotating the electron diamagnetic direction. As n increases, the real frequency crosses $\omega_r = 0$ and becomes negative values, i.e. the ion-diamagnetic direction, indicating that the TEMs are thought to transit to ubiquitous modes, which is the non-resonant counterpart of TEMs, but rotate in the ion diamagnetic direction [15][16]. Furthermore, they tend to pure toroidal ITG modes [17]. Meanwhile, the latter branch is the slab-like non-resonant ITG modes, which show the largest growth rate at n = 28. The radial location of each mode is mapped in the plain of $(R_0/L_T, R_0/L_n)$ as shown in Fig. 1(e). The boundary of inner and outer branches can be seen in the region of $\eta_i = 2 \sim 4$, which is mapped inside the q_{min} surface at r = 0.6. It is noted that each branch is found to have nearly the same maximum values for the growth rate in inner and outer regions, i.e. $\gamma_{max}^{in} \sim \gamma_{max}^{out}$, indicating that linearly unstable free energy sources are organized to be globally balanced so as not to cause unbalanced transport between inner and outer regions. This is considered to be a global version of such marginal stability.

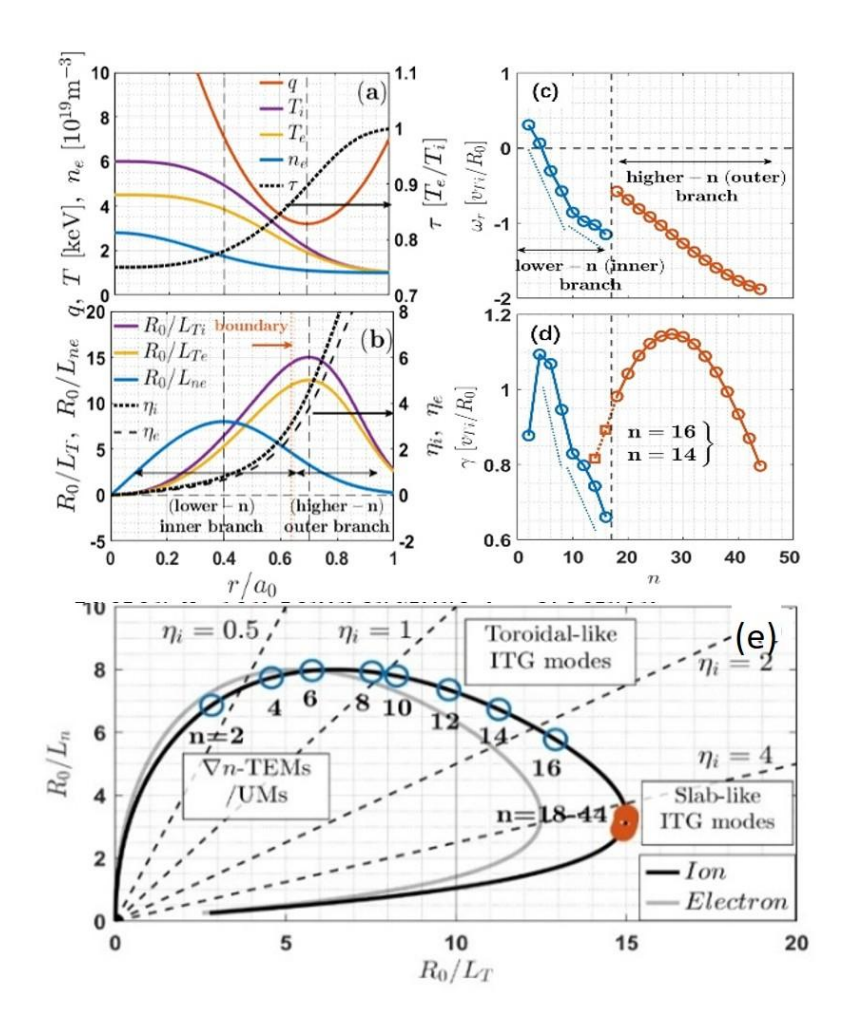


Fig. 1 (a) Equilibrium profiles of the safety factor q, ion temperature T_i , electron temperature T_e , electron density n_e , and τ defined by T_e/T_i ; (b) Inverse normalized scale length profiles (R/L) of T_i , T_e , and n_e ; (c), (d) The dispersion relation of the real frequency ω_r , growth rate γ to the toroidal mode number n. (e) Mode location in the parameter space of $(R_0/L_T, R_0/L_n)$.

4. NONLINEAR TURBULENCE SIMULATION

Figure 2 illustrates the time evolution of (a) the radial distribution of the ion heat flux, $Q_i(r,t)$, and (b) the space-averaged ion heat flux, $Q_i(t)$. The time history is divided into three phases: Phase-(I) $27 \le t \le 35$, Phase-(II) $35 < t \le 60$, and Phase-(III) $60 < t \le 120$. Similarly, three radial domains are defined as: [A] the inside region $0 \le r < 0.34$, [B] the intermediate region $0.34 \le r \le 0.70 = r_{min}$, and [C] the outside region of the q_{min} surface, i.e., $0.70 < r \le 1$, as shown in Fig. 2.

After the linear growth stage (up to t=27), the system enters the nonlinear growth phase, as Phase-(I), where the nonlinear interactions become dominant and drive heat transport. As indicated by the linear analysis, the mode for n=4 in the inner branch and n=28 in the outer branch, each exhibiting the largest growth rate in its respective region, begin to grow nearly simultaneously from $r=r_{in}(=0.34)$ and $r=r_{min}(=0.7)$ at $t\sim27$. Fig. 3(a) shows the turbulent potential structures at t=27, in which the linear mode structures are still retained. These modes then develop into turbulence, spreading both radially inward and outward, as illustrated in Fig. 3(b). the turbulence also spreads poloidally, but still shows features biased towards the outside bad curvature region of $|\theta| \leq \pi/2$. Subsequently, they merge and interact around the interface between the two branches (r=0.6), as Fig. 3(c) shows.

In Phase-(II), a strong burst occurs and persists from $t \sim 35$ to $t \sim 60$, characterized by a mesh-like avalanche pattern with the opposite phase velocities. Owing to the inverse cascade, low-n modes in region [B] with relatively larger q values become dominant, forming large-scale eddies that enhance heat transport. In Phase-

(III), the system evolves into a quasi-steady state with several small bursting events, the space-averaged amplitude of which is lower than that in the Phase-(II). The radial distribution of $Q_i(r,t)$ develops distinct transport boundaries at $r_{in} \sim 0.2$ and $r_{out} \sim 0.8$. The persistence of a strongly reversed shear q profile near the plasma core and edge is considered one of the key factors responsible for the formation of these transport boundaries.

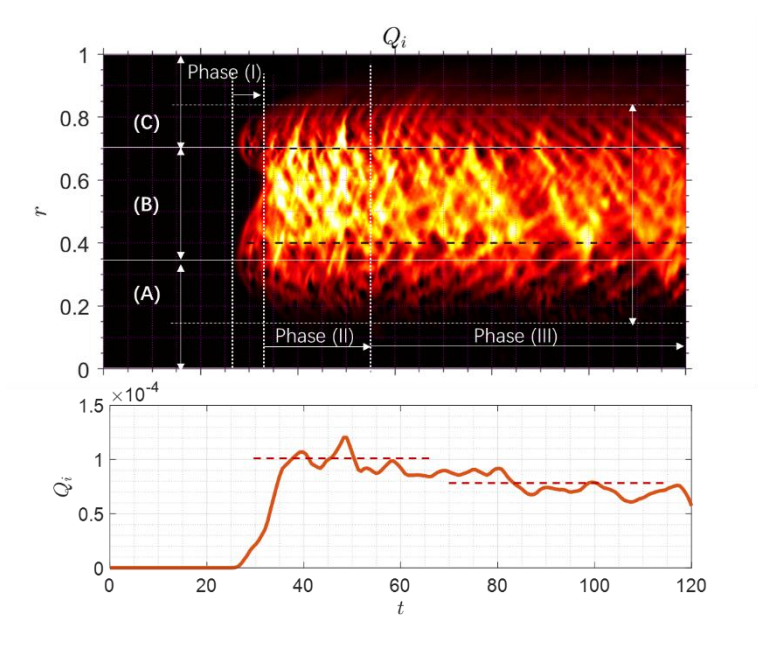


FIG. 2 The time evolution of the radial distribution of ion heat flux $Q_i(r,t)$ (up), and the space-averaged ion heat flux $Q_i(t)$ (down).

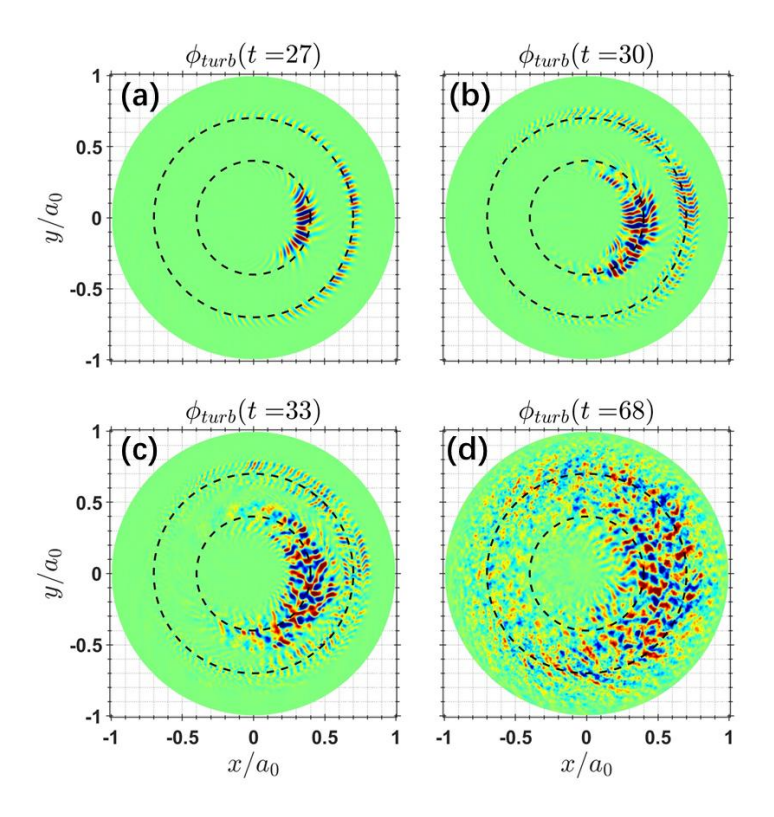


FIG. 3 The two-dimensional electrostatic potential distribution $\phi(x, y)$ at (a) t = 28, (b) t = 30, (c) t = 33, and (d) t = 68, respectively.

Owing to the relatively high q value in the system, geodesic acoustic modes (GAMs) can be easily excited [18]. Fig. 4 presents the time evolution of the radial electric field E_r , showing a pronounced oscillatory feature that can be attributed to geodesic acoustic modes (GAMs) [19]-[22]. By decomposing $E_r(t)$ into a quasi-steady part $\overline{E_r}(t)$, and a fluctuation part $\delta E_r(t)$, we found that the fluctuation amplitude $\delta E_r(t)$ comparable in magnitude to $\overline{E_r}(t)$. This result indicate that GAMs constitute one of the dominant components of the radial electric field. Furthermore, the frequency spectrum of δE_r lies within the typical GAM frequency range. However, the observed frequency exhibits little radial variation, especially near the q_{min} region, suggesting the presence of a radially global mode. Such structures are interpreted as global GAMs [20].

The time evolution of E_r exhibits structures similar to those of Q_i , allowing both time and space to be divided into three domains, respectively. The self-generated E_r radial shear profile $(\partial_r E_r)$ can also be decomposed into the quasi-steady component $\partial_r \overline{E_r}$, and the fluctuation component $\delta \partial_r E_r$. A large variation of $\overline{E_r}(t)$ around the boundaries of region [B] (near r=0.34 and r=0.7) forms a stable shearing layer with two local maxima, which is clearly visible in $\partial_r \overline{E_r}$ evolution subgraph. These shearing layers distort turbulent eddies, thereby reducing their radial correlation length and suppressing effective transport across the plasma. In contrast to $\delta E_r(t)$ and $\overline{E_r}(t)$, whose amplitudes are comparable, the amplitude of $\delta \partial_r E_r$ is nearly one order of magnitude larger than that of $\partial_r \overline{E_r}$, indicating that GAMs play an important role in this system. After entering Phase-(III), the quasi-steady state, well-organized structures of $\delta \partial_r E_r$ with opposite phase velocities appear in regions [A] and [C]. This behavior arises because the turbulence energy excited around the q_{min} surface is transferred to propagating GAMs [21]. The associated oscillations in E_r and $\partial_r E_r$ are advected beyond the q_{min} surface and dissipated into the plasma, thereby suppressing turbulence.

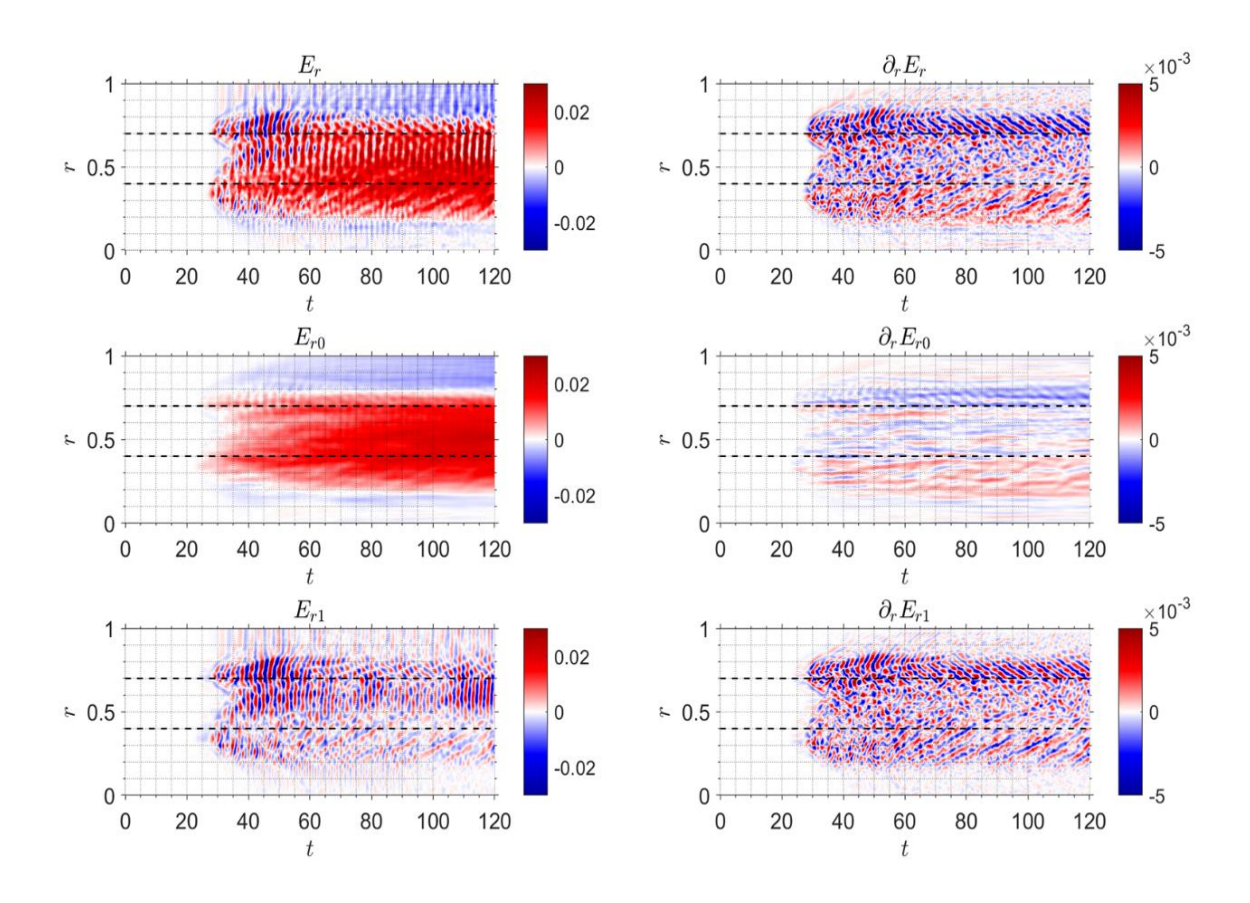


FIG. 4 The time evolution of the radial electric field E_r , its quasi-static component E_{r0} and oscillation component E_{r1} , and the corresponding radial gradient $\partial_r E_r$, $\partial_r E_{r0}$, and $\partial_r E_{r1}$.

Correspondingly, the poloidally $E \times B$ shear flow, with two maxima located on the inside and outside of the plasmas, restricts the radial spreading of the heat flux in these regions, thereby forming certain heat flux boundaries at $r_{in} \sim 0.2$ and $r_{out} \sim 0.8$, as shown in Fig. 2(a) and (b). In Fig. 5(a), the $E \times B$ shearing rate [23][24] is calculated from the radial electric field E_r from Fig. 4 as

$$\omega_{E \times B} = \frac{r}{q} \frac{\partial}{\partial r} \left(\frac{q}{r} \frac{E_r}{B_{\phi}} \right). \tag{4}$$

Owing to the large $\partial_r E_r$, the amplitude of $\omega_{E\times B}$ (blue dotted line) can reach values four or five times higher than the maximum linear growth rate obtained from the linear simulations in Fig. 1(d), as indicated by the red line. However, because the fluctuating shear flow associated with GAMs has a finite oscillation frequency, the effective shearing rate ω_{eff} should be reduced, as expressed by the formulation in [25]

$$\omega_{eff} = \omega_{E \times B} H,\tag{5}$$

where $H(F) \le 1$ is the oscillatory reduction factor, and $F = \omega_f^2/\Delta\omega_T^2$ represents the square ratio of the fluctuating flow frequency to the turbulence decorrelation rate. The reduction factor accounts for the fact that the oscillatory nature of GAM-modulated flows limits their instantaneous effectiveness in suppressing turbulence. Even after accounting for this reduction, ω_{eff} remains sufficiently large, comparable to the maximum linear growth rate and exceeding it in the outer region of q_{min} , indicating that turbulence suppression is still effective despite the flow oscillations, as illustrated by the black line in Fig. 5(a).

During this transport process, the system evolves into a quasi-stationary state, characterized by semi-globally relaxation of the profiles. The inner barrier corresponds to the region of maximum density gradient, where turbulence is suppressed by the combined action of quasi-steady and fluctuating $E \times B$ shears, while the outer barrier forms near the q_{min} surface, where GAM-modulated flows further stabilize the plasma. These observations suggest that two ITBs are primed to be triggered, one outside the q_{min} surface and the other inside the maximum density gradient region (Fig. 5(b)). In other words, a nascent double-barrier structure can emerge if the input heating power is sustained, providing favourable conditions for enhanced confinement.

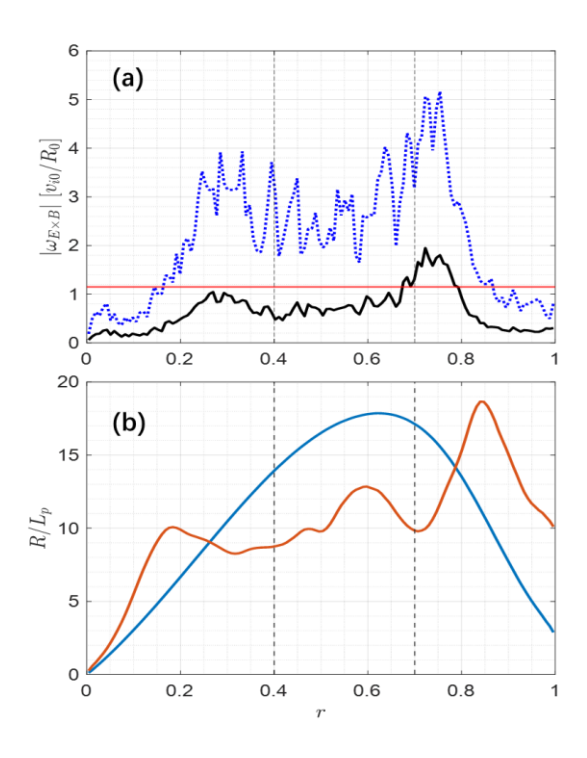


FIG. 5 (a) The effective $E \times B$ shearing rate ω_{eff} (black line) and the initial shear rate $\omega_{E \times B}$ (blue dotted line); (b) The pressure normalized inverse scale length profile at initial stage (blue line) and quasi-steady stage (red line).

5. CONCLUSIONS

We investigated the characteristics of L-mode plasmas exhibiting two spatially separated free energy sources in the inner and outer regions, each with approximately comparable linear growth rate, modeled for JT-60U strong RS discharges under strong profile constraints below the critical power P_c , above which ITBs are known to be triggered. Under the hypothesis that signs of an ITB trigger may already exist in such L-mode plasmas, we performed δf -based gyro-kinetic simulations leading to the first-order redistribution of profiles induced by turbulence, while the system remained in the L-mode state. Our simulations reveal that global turbulence coupled with GAMs and resultant reduced transport are observed in both inner and outer regions, corresponding to the free energy sources localized at $r \sim 0.34$ and $r \sim 0.7 (= r_{min})$, respectively. The turbulence is characterized by a smaller number of lower n modes dominated by larger scale eddies in the inside region, whereas the outer region is dominated by a larger number of higher n modes and smaller scales. These structures induce redistribution of profiles, forming two localized suppression layers: one is the inside region with a steep density gradient, and the other is outside the q_{min} surface. These two layers are anticipated to serve as seeds for triggering ITBs when the input power is sufficiently high. Furthermore, global effects arising from the variation of profiles under weak or vanishing magnetic shear play a crucial role, which cannot be captured by local analyses alone. Such global coupling highlights the importance of considering both radial profile variations and turbulence-GAM interactions in understanding the early stages of ITB formation.

ACKNOWLEDGEMENTS

The authors would like to thank Dr. F. Kin, Dr. K. Nagasaki, and Dr. E. Narita in Kyoto University, Dr. N. Aiba, Dr. M. Yoshida, and Dr. M. Yagi in QST, Dr. J.Y. Kim in KFE, Dr. H.T. Chen, Dr. G.Z. Hao, Dr. W. Chen, and Dr. D.L. Yu in SWIP for their valuable comments on this study. This work is performed on the 'Plasma Simulator' (NEC SX-Aurora TSUBASA) of NIFS with the support and under the auspices of the NIFS Collaboration Research program (NIFS22KIST008). This work was financially supported by the National Key R&D Program of China (Grant No. 2024YFE03160003), National Natural Science Foundation of China (Grant No. 12205080), and the China Scholarship Council (Grant No. 202106060080).

REFERENCES

- [1] Connor, J. W., et al. "A review of internal transport barrier physics for steady-state operation of tokamaks." Nucl. Fusion 44.4 (2004): R1.
- [2] Ida, Katsumi, and Takaaki Fujita. "Internal transport barrier in tokamak and helical plasmas." Plasma Phys. Control. Fusion 60.3 (2018): 033001.
- [3] Ishida, S., et al. "Achievement of high fusion performance in JT-60U reversed shear discharges." Phys. Rev. Lett. 79.20 (1997): 3917.
- [4] Fujita, Takaaki, et al. "Internal transport barrier for electrons in JT-60U reversed shear discharges." Phys. Rev. Lett. 78.12 (1997): 2377.
- [5] Kin, F., et al. "Impact of avalanche type of transport on internal transport barrier formation in tokamak plasmas." Sci. Rep. 13.1 (2023): 19748.
- [6] Kin, F., et al. "Experimental evaluation of avalanche type of electron heat transport in magnetic confinement plasmas." Nucl. Fusion 63.1 (2022): 016015.
- [7] Imadera, K., et al. "Global profile relaxation coupled with E x B staircase in toroidal flux-driven ITG turbulence." 25th IAEA Int. Conf. on Fusion Energy. 2014.
- [8] Imadera, K., and Kishimoto, Y. "ITB formation in gyrokinetic flux-driven ITG/TEM turbulence." Plasma Phys. Controlled Fusion 65.2 (2022): 024003.
- [9] Imadera, K., Kishimoto, Y. and Ishizawa, A. "Turbulent particle pinch in gyrokinetic flux-driven ITG/TEM turbulence." Nucl. Fusion 64.8 (2024): 086006.
- [10] Zhao, R., et al. "Characteristics of global dispersion and mode distribution modeled for JT-60U like strongly reversed magnetic shear plasmas exhibiting L-modes with strong profile constraints." Nucl. Fusion 65.5 (2025): 056037.
- [11] Lanti, E., et al. "Gradient-and flux-driven global gyrokinetic simulations of ITG and TEM turbulence with an improved hybrid kinetic electron model." J. Phys.: Conf. Ser. Vol. 1125. No. 1. IOP Publishing, 2018.
- [12] Idomura, Y. "A new hybrid kinetic electron model for full-f gyrokinetic simulations." J. Comput. Phys. 313 (2016): 511-531.

[Right hand page running head is the paper number in Times New Roman 8 point bold capitals, centred]

- [13] Adam, J. C., W. M. Tang, and P. H. Rutherford. Destabilization of the trapped electron mode by magnetic curvature drift resonances. No. MATT-1156. Princeton Plasma Physics Lab. (PPPL), Princeton, NJ (United States), 1975.
- [14] Romanelli, F., and S. Briguglio. "Toroidal semicollisional microinstabilities and anomalous electron and ion transport." Physics of Fluids B: Plasma Physics 2.4 (1990): 754-763.
- [15] Coppi, B., and Francesco Pegoraro. "Theory of the ubiquitous mode." Nucl. Fusion 17.5 (1977): 969.
- [16] Choudhary, Sagar, et al. "Global gyrokinetic study of density gradient driven instability in tokamaks: the ubiquitous mode." Plasma Phys. Control. Fusion 66.8 (2024): 085013.
- [17] Kim, J. Y., and H. S. Han. "Linear interaction and relative role of the ion temperature gradient and trapped electron modes in the reactor-relevant finite beta plasma condition." Phys. Plasmas 24.7 (2017).
- [18] Conway, Garrard D., Andrei I. Smolyakov, and Takeshi Ido. "Geodesic acoustic modes in magnetic confinement devices." Nucl. Fusion 62.1 (2021): 013001.
- [19] Miyato, Naoaki, Yasuaki Kishimoto, and Jiquan Li. "Global structure of zonal flow and electromagnetic ion temperature gradient driven turbulence in tokamak plasmas." Phys. Plasmas 11.12 (2004): 5557-5564.
- [20] Miyato, N., Y. Kishimoto, and J. Q. Li. "Turbulence suppression in the neighbourhood of a minimum-q surface due to zonal flow modification in reversed shear tokamaks." Nucl. Fusion 47.8 (2007): 929.
- [21] Miki, K., et al. "Intermittent Transport Associated with the Geodesic Acoustic Mode near the Critical Gradient Regime." Phys. Rev. Lett 99.14 (2007): 145003.
- [22] Sasaki, M., et al. "Transient excitation of zonal flows by geodesic acoustic modes." Plasma Phys. Control. Fusion 51.8 (2009): 085002.
- [23] Hahm, T. S., and K. H. Burrell. "Flow shear induced fluctuation suppression in finite aspect ratio shaped tokamak plasma." Phys. Plasmas 2.5 (1995): 1648-1651.
- [24] Waltz, R. E., and R. L. Miller. "Ion temperature gradient turbulence simulations and plasma flux surface shape." Phys. Plasmas 6.11 (1999): 4265-4271.
- [25] Hahm, T. S., et al. "Shearing rate of time-dependent E×B flow." Phys. Plasmas 6.3 (1999): 922-926.